

Thermodynamics of a spin-1 Bose gas with fixed magnetization

Guillaume Lang and Emilia Witkowska

Instytut Fizyki PAN, Aleja Lotników 32/46, 02-668 Warsaw, Poland

We investigate the thermodynamics of a spin-1 Bose gas with fixed magnetization including the quadratic Zeeman energy shift. Our calculations are based on the grand canonical description for the ideal gas and the classical fields approximation for atoms with ferromagnetic and antiferromagnetic interactions. We confirm the occurrence of a double phase transition in the system that takes place due to two global constraints. We show analytically for the ideal gas how critical temperatures and condensed fractions are changed by a non-zero magnetic field. The interaction strongly affects the condensate scenario below the second critical temperature. The effect imposed by interaction energies becomes diminished in high magnetic fields where condensation, of both ferromagnetic and antiferromagnetic atoms, agree with the ideal gas results.

PACS numbers: 03.75.Mn, 05.30.-d, 05.70.Fh, 03.50.-z,

I. INTRODUCTION

A spinor Bose-Einstein condensate (BEC) is a multi-component condensate with an additional spin degree of freedom, which has provided exciting opportunities to study experimentally quantum magnetism, superfluidity, strong correlations, coherent spin-mixing dynamics, spin-nematic squeezing, entanglement etc, most of them in non-equilibrium situations (see [1–6]). Despite successful experimental developments on spinor Bose-Einstein condensates, our knowledge remains limited regarding equilibrium properties and in particular the thermodynamics of such a gas. The main reason is a long time needed to reach an equilibrium state, typically several seconds or tens of seconds, that may exceed the lifetime of the condensate [7]. Nevertheless, recent experimental developments allowed for investigation of the ground state of an antiferromagnetic spinor condensate opening the paths to study in details its properties at thermal equilibrium [8].

The condensation of atoms with total spin $F = 1$ trapped in the three hyperfine states $m_F = 1, 0, -1$ in the absence of magnetic field was investigated theoretically for the first time by Isoshima et al. [9]. The double condensation phenomenon was predicted in the presence of two global conserved quantities: the total number of atoms N and the magnetization M . A condensate starts to appear in the highest $m_F = 1$ component for temperatures below the first critical temperature and simultaneously in the rest two components for temperatures below the second critical temperature. Analytical expressions for the two critical temperatures and condensate fractions were given for the ideal gas and zero magnetic field [9, 10]. The condensation of interacting spin-1 Bose gas was considered numerically within the Bogoliubov-Popov approximation [9] and the Hartree-Fock-Popov approximation [11]. In the latter, authors confirmed the double phase transition for antiferromagnetic interactions, but found a more complicated phase diagram for ferromagnetic interactions with a possible triple condensation scenario. The only one experimental

work of Pasquiou [12] touches the problem of the thermodynamics in chromium atoms with total spin $F = 3$ but for free magnetization. Indeed, for low magnetic fields when the magnetization is approximately conserved the experimental results confirm the occurrence of a double condensation.

In this paper, we reconsider the topic of condensation in the system of spin-1 bosons with fixed magnetization. The ultra-cold gases are almost perfectly isolated in the experiment and conservation of magnetization plays a major role. The magnetic dipole-dipole interactions, that may change the magnetization, are relatively weak and can be neglected for $F = 1$ sodium or rubidium spinor Bose-Einstein condensates.

We examine the thermodynamics of the ideal gas in the presence of quadratic Zeeman effect within the grand canonical ensemble. A non-zero magnetic field introduces a new phase in the phase diagram of critical temperatures that we characterize by the threshold magnetization. The condensation scenario predicted by Isoshima is present for magnetizations larger than the threshold magnetization. When the magnetization of the system is smaller than the threshold magnetization, atoms start condensing first not in the highest $m_F = 1$ component, as it was the case for zero magnetic field, but in the $m_F = 0$ component. That trivial effect is present due to the shift of the lowest energy level of the $m_F = 0$ component below the lowest energy level of the $m_F = 1$ component. We give an explicit expression for the threshold magnetization.

We study the interacting gas within the classical fields approximation [13] combined with the Metropolis algorithm [14]. The method was successfully used to investigate thermal effects in the single-component Bose-Einstein condensates including thermodynamics [15], vortex-dynamics [16], critical temperature shift [17], spin-squeezing [18], solitons or Kibble-Zurek mechanism [19], and many others, some of them reviewed in [20]. This numerical method includes all non-linear terms present in the Hamiltonian at the expense of introducing a free parameter that has to be well chosen. In this paper we explain how to adapt the Metropolis

algorithm for a spin-1 gas with fixed magnetization. To demonstrate the validity of the proposed algorithm we compared results of simulations with exact results for the ideal gas and with the approximated Bogoliubov theory for antiferromagnetic interactions. We confirmed double condensation for both ferromagnetic and antiferromagnetic interactions. The condensation strongly differs from the result for ideal gas below the second critical temperature. In the high magnetic field limit, when the quadratic Zeeman energy dominates over the interaction energy, details of condensation do not depend on the interaction sign and are well described by the ideal gas results.

II. THE MODEL

We consider a dilute and homogeneous spin-1 Bose gas in a magnetic field. We start with the Hamiltonian $H = H_0 + H_A$, where the symmetric (spin-independent) part is

$$H_0 = \sum_{j=-,0,+} \int d^3r \psi_j^\dagger \left(-\frac{\hbar^2}{2m} \nabla^2 + \frac{c_0}{2} n \right) \psi_j. \quad (1)$$

Here the subscripts $j = -, 0, +$ denote sublevels with magnetic quantum numbers along the magnetic field axis $m_F = -1, 0, +1$, m is the atomic mass, $n = \sum_j n_j = \sum_j \psi_j^\dagger \psi_j$ is the total atom density. The spin-dependent part can be written as

$$H_A = \int d^3r \left[\sum_j E_j n_j + \frac{c_2}{2} : \mathbf{F}^2 : \right], \quad (2)$$

where E_j are Zeeman energy levels, $\mathbf{F} = (\psi^\dagger f_x \psi, \psi^\dagger f_y \psi, \psi^\dagger f_z \psi)^T$ is the spin density, $f_{x,y,z}$ are spin-1 matrices, $\psi = (\psi_+, \psi_0, \psi_-)^T$, and $::$ denotes the normal order. The spin-independent and spin-dependent interaction coefficients are given by $c_0 = 4\pi\hbar^2(a_0 + 2a_2)/3m$ and $c_2 = 4\pi\hbar^2(a_2 - a_0)/3m$ respectively, where a_S is the s-wave scattering length for colliding atoms with total spin S . The total number of atoms

$$N = \int n d^3r \quad (3)$$

and the magnetization

$$M = \int (n_+ - n_-) d^3r \quad (4)$$

are conserved quantities.

The linear part of the Zeeman shifts E_j induces a homogeneous rotation of the spin vector around the direction of the magnetic field. Since the Hamiltonian is invariant with respect to such spin rotations, we consider only the effect of the quadratic Zeeman shift.

For a sufficiently weak magnetic field we can approximate Zeeman energy levels by a positive energy shift of the $m_F = \pm 1$ sublevels $\delta = (E_+ + E_- - 2E_0)/2 \approx qh^2$, where h is the magnetic field strength and $q = (g_I + g_J)^2 \mu_B^2 / 16 E_{\text{HFS}}$, g_I and g_J are the gyromagnetic ratios of the electron and the nucleus, μ_B is the Bohr magneton, E_{HFS} is the hyperfine energy splitting at zero magnetic field. Finally, the spin-dependent Hamiltonian (2) becomes

$$H_A = \int d^3r \left[qh^2(n_+ + n_-) + \frac{c_2}{2} : \mathbf{F}^2 : \right], \quad (5)$$

where $F_z^2 = n_+ - n_-$ and $F_\perp^2 = 2|\psi_+ \psi_0^\dagger + \psi_0 \psi_-^\dagger|^2$ are the square of magnetization density and the square of transverse spin density, respectively. In spinor condensates realized in laboratories, a_0 and a_2 scattering lengths have similar magnitude. The spin-dependent interaction coefficient c_2 is, therefore, much smaller than its spin-independent counterpart c_0 . For ^{23}Na condensate their ratio is about 1:30 and is positive (antiferromagnetic order), while for ^{87}Rb condensate it is 1:220 and is negative (ferromagnetic order).

By comparing the kinetic energy with the interaction energy, we can define the healing length $\xi = 2\pi\hbar/\sqrt{2mc_0n}$ and the spin healing length $\xi_s = 2\pi\hbar/\sqrt{2mc_2n}$. These quantities give the length scales of spatial variations in the condensate profile induced by the spin-independent or spin-dependent interactions. Here we consider system sizes smaller than the spin healing length in order to avoid a domain formation. A good basis for such a homogeneous system is the plane wave basis.

III. THE IDEAL GAS

We consider a uniform gas of non-interacting atoms ($c_0 = c_2 = 0$) with hyperfine spin $F = 1$ in a homogeneous magnetic field h within the grand canonical ensemble, taking into account the quadratic Zeeman effect. The effective Hamiltonian of the system is

$$H_{eff} = \sum_{m_F=1,0,-1} \sum_{\mathbf{k}} (\epsilon_{\mathbf{k}} + m_F^2 qh^2) n_{\mathbf{k},m_F} - \mu N - \eta M, \quad (6)$$

with

$$N = N_+ + N_0 + N_- = \sum_{m_F} \sum_{\mathbf{k}} n_{\mathbf{k},m_F}, \quad (7)$$

$$M = N_+ - N_- = \sum_{m_F} \sum_{\mathbf{k}} m_F n_{\mathbf{k},m_F}. \quad (8)$$

Here $\mathbf{k} = 2\pi/L(n_x, n_y, n_z)$, L is the system size and $n_l = 0, \pm 1, \pm 2 \dots$ are integers, $n_{\mathbf{k},m_F}$ are occupation numbers of atoms of energy $\epsilon_{\mathbf{k}} = \hbar^2 \mathbf{k}^2 / 2m$. The chemical potential μ and the linear Zeeman shift η are Lagrange multipliers enforcing the desired total atom number N and the magnetization M respectively. N_{m_F} is the number of atoms in the m_F th component. We consider a

positive magnetization $M \geq 0$ and a positive Zeeman energy shift $qh^2 > 0$.

The non-zero magnetic field removes the degeneracy of energy spectra:

$$E_{\mathbf{k},+} = \epsilon_{\mathbf{k}} - \mu - \eta + qh^2, \quad (9)$$

$$E_{\mathbf{k},0} = \epsilon_{\mathbf{k}} - \mu, \quad (10)$$

$$E_{\mathbf{k},-} = \epsilon_{\mathbf{k}} - \mu + \eta + qh^2. \quad (11)$$

The ratio between η and qh^2 determines the order of energy levels. The lowest energy level is E_+ for $qh^2 \leq \eta$, or E_0 for $qh^2 \geq \eta$. In addition, two effects determine the state of the system: (i) the occupation number imbalance enforced by the fixed magnetization $N_+ \geq N_-$, and (ii) the ground state energy level (E_0 or E_+) controlled by the magnetic field.

Since the Hamiltonian is diagonal, we may calculate the grand canonical partition function

$$\Xi = \sum_{m_F, n_{\mathbf{k}, m_F}} e^{-\beta E_{\mathbf{k}, m_F} n_{\mathbf{k}, m_F}}, \quad (12)$$

where $\beta = 1/k_B T$, T is the temperature and k_B is the Boltzmann constant. The ensemble average of the occupation number $n_{\mathbf{k}, m_F}$ is

$$n_{\mathbf{k}, m_F} = -\frac{1}{\beta} \frac{\partial \ln \Xi}{\partial E_{\mathbf{k}, m_F}}, \quad (13)$$

which gives

$$n_{\mathbf{k}, m_F} = \frac{z_{m_F} e^{-\beta \epsilon_{\mathbf{k}}}}{1 - z_{m_F} e^{-\beta \epsilon_{\mathbf{k}}}} \quad (14)$$

with effective fugacities

$$z_+ = e^{\beta(\mu + \eta - qh^2)}, \quad (15)$$

$$z_0 = e^{\beta \mu}, \quad (16)$$

$$z_- = e^{\beta(\mu - \eta - qh^2)}. \quad (17)$$

In the thermodynamic limit, keeping only dominant terms $O(N)$, expressed in terms of fugacities, the number of atoms in the lowest energy level of each m_F component is

$$N_{m_F}^c = \frac{z_{m_F}}{1 - z_{m_F}}, \quad (18)$$

while the number of thermal atoms in each m_F component is

$$N_{m_F}^T = \left(\frac{L}{\lambda_{dB}} \right)^3 g_{\frac{3}{2}}(z_{m_F}), \quad (19)$$

where $\lambda_{dB} = h/\sqrt{2\pi m k_B T}$ is the de Broglie wave length, and $g_j(x) = \sum_{n=1}^{+\infty} x^n/n^j$ is the Bose function.

A. Transition temperatures and condensate fractions

1. For $qh^2 \leq \eta$

The first phase transition occurs for $z_+ \rightarrow 1$ (or $\mu \rightarrow qh^2 - \eta$) when the $m_F = 1$ component starts condensing. That $N_+^c \gg 1$ can be seen from (18). The number of thermal atoms is then

$$N_+^T = \left(\frac{L}{\lambda_{dB}} \right)^3 g_{\frac{3}{2}}(1), \quad (20)$$

$$N_0^T = \left(\frac{L}{\lambda_{dB}} \right)^3 g_{\frac{3}{2}}(e^{\beta qh^2} z_\eta), \quad (21)$$

$$N_-^T = \left(\frac{L}{\lambda_{dB}} \right)^3 g_{\frac{3}{2}}(z_\eta^2), \quad (22)$$

with $z_\eta \equiv e^{-\beta \eta}$. The first critical temperature T_{c1} can be obtained from the following equations:

$$N = \left(\frac{L}{\lambda_{dB}(T_{c1})} \right)^3 F_{\frac{3}{2}}^+(T_{c1}, z_{\eta c1}), \quad (23)$$

$$M = \left(\frac{L}{\lambda_{dB}(T_{c1})} \right)^3 \left(g_{\frac{3}{2}}(1) - g_{\frac{3}{2}}(z_{\eta c1}^2) \right), \quad (24)$$

where we have introduced the notation $z_{\eta c1} \equiv z_\eta(T_{c1})$ and

$$F_{\frac{3}{2}}^+(T, z_\eta) \equiv g_{\frac{3}{2}}(1) + g_{\frac{3}{2}}(e^{\beta qh^2} z_\eta) + g_{\frac{3}{2}}(z_\eta^2). \quad (25)$$

Below T_{c1} , only the $m_F = 1$ component condenses. It is justified to assume $N_+^c \simeq N^c$. Then relation $N^c = N - \sum_\sigma N_\sigma^T$ defines the condensate fraction of the $m_F = 1$ component

$$\frac{N_+^c}{N} \simeq 1 - \left(\frac{T}{T_{c1}} \right)^{\frac{3}{2}} \frac{F_{\frac{3}{2}}^+(T, z_\eta)}{F_{\frac{3}{2}}^+(T_{c1}, z_{\eta c1})}. \quad (26)$$

The second phase transition occurs for $z_\eta \rightarrow e^{-\beta qh^2}$ ($\eta \rightarrow qh^2$) when $N_0^c \gg 1$ and $N_-^c \rightarrow e^{-2\beta qh^2}/(1 - e^{-2\beta qh^2})$. In this regime, $T < T_{c2}$, thermal populations are

$$N_+^T = \left(\frac{L}{\lambda_{dB}} \right)^3 g_{\frac{3}{2}}(1), \quad (27)$$

$$N_0^T = \left(\frac{L}{\lambda_{dB}} \right)^3 g_{\frac{3}{2}}(1), \quad (28)$$

$$N_-^T = \left(\frac{L}{\lambda_{dB}} \right)^3 g_{\frac{3}{2}}(e^{-2\beta qh^2}). \quad (29)$$

The second transition temperature T_{c2} can be obtained using the difference between the total atom number N and the magnetization M . For temperatures $T \in [T_{c2}, T_{c1}]$, in the absence of condensates in $m_F = 0, -1$ components, the difference is $N - M \simeq 2N_+^T + N_0^T$. The

second transition temperature expressed in terms of Bose functions present in equations (21) and (22) is

$$k_B T_{c2} = \frac{2\pi\hbar^2}{mL^2} \left[\frac{N-M}{G_{\frac{3}{2}}(T_{c2})} \right]^{\frac{2}{3}}, \quad (30)$$

where

$$G_{\frac{3}{2}}(T) \equiv g_{\frac{3}{2}}(1) + 2g_{\frac{3}{2}}(e^{-2\beta qh^2}). \quad (31)$$

Below T_{c2} , the Bose-Einstein condensate can be formed in all components and condensate fractions satisfy the set of equations:

$$\begin{aligned} N^c &= M^c(T) + (N-M) \left[1 - \left(\frac{T}{T_{c2}} \right)^{\frac{3}{2}} \frac{G_{\frac{3}{2}}(T)}{G_{\frac{3}{2}}(T_{c2})} \right], \\ N_+^c - N_-^c &= M^c(T), \\ \frac{2}{N_0^c} &= \frac{1}{N_+^c} + \frac{e^{-2\beta qh^2}}{N_-^c} - 2 \sinh(\beta qh^2) e^{-\beta qh^2}. \end{aligned} \quad (32)$$

Here we have introduced the condensate part of the magnetization $M^c \equiv M - M^T$ and the thermal part of magnetization

$$M^T(T) \equiv \left(\frac{L}{\lambda_{dB}} \right)^3 \left[g_{\frac{3}{2}}(1) - g_{\frac{3}{2}}(e^{-2\beta qh^2}) \right]. \quad (33)$$

A derivation of eqs. (32) is included in Appendix A. An analytical solution of eqs. (32) is presented in Appendix B. We have checked the validity of the analytical solution against the self-consistent numerical result.

2. For $qh^2 \geq \eta$

First, one should notice that this case does not exist in the absence of an external magnetic field, since η can take positive values for $M > 0$. That is a new area of the phase diagram, which appears due to the quadratic Zeeman effect.

The first phase transition. This time, the $m_F = 0$ component undergoes condensation first, which means that $z_0 \rightarrow 1$ (or $\mu \rightarrow 0$) and $N_0^c \gg 1$. One obtains new expressions for N_+^T , N_0^T and N_-^T , which hold under the critical temperature T_{c1} :

$$N_+^T = \left(\frac{L}{\lambda_{dB}} \right)^3 g_{\frac{3}{2}}(e^{-\beta qh^2} z_\eta^{-1}), \quad (34)$$

$$N_0^T = \left(\frac{L}{\lambda_{dB}} \right)^3 g_{\frac{3}{2}}(1), \quad (35)$$

$$N_-^T = \left(\frac{L}{\lambda_{dB}} \right)^3 g_{\frac{3}{2}}(e^{-\beta qh^2} z_\eta). \quad (36)$$

The first critical temperature T_{c1} and the fugacity at the critical point $z_{\eta c1}$ can be obtained from the following

equations:

$$\begin{aligned} N &= \left(\frac{L}{\lambda_{dB}(T_{c1})} \right)^3 F_{\frac{3}{2}}^0(T_{c1}, z_{\eta c1}), \\ M &= \left(\frac{L}{\lambda_{dB}(T_{c1})} \right)^3 \left[g_{\frac{3}{2}}(z_{\eta c1}^{-1} e^{-\frac{\beta qh^2}{kT_{c1}}}) - g_{\frac{3}{2}}(z_{\eta c1} e^{-\frac{\beta qh^2}{kT_{c1}}}) \right], \end{aligned} \quad (37)$$

where we have introduced

$$F_{\frac{3}{2}}^0(T, z_\eta) \equiv g_{\frac{3}{2}}(z_\eta^{-1} e^{-\beta qh^2}) + g_{\frac{3}{2}}(1) + g_{\frac{3}{2}}(z_\eta e^{-\beta qh^2}). \quad (39)$$

At the critical the point the fugacity is smaller than one ($z_\eta(T_{c1}) < 1$) since $M \geq 0$ and $g_{\frac{3}{2}}$ is an increasing function of its argument and takes positive values.

Assuming that $N_0^c \simeq N^c$ for $T \in [T_{c2}, T_{c1}]$, once again the relation $N^c = N - \sum_{m_F} N_{m_F}^T$ defines the condensate fraction in the $m_F = 0$ component

$$\frac{N_0^c}{N} \simeq 1 - \left(\frac{T}{T_{c1}} \right)^{\frac{3}{2}} \frac{F_{\frac{3}{2}}^0(T, z_\eta)}{F_{\frac{3}{2}}^0(T_{c1}, z_{\eta c1})}. \quad (40)$$

The second phase transition. One expects $z_\eta \sim e^{-\beta qh^2}$, implying that the $m_F = 1$ component starts condensing: $N_+^c \gg 1$ and again $N_-^c \rightarrow e^{-2\beta qh^2}/(1 - e^{-2\beta qh^2})$. Nevertheless, in this regime we should define T_{c2} in the other way. Neither N nor $N - M$ can be used anymore, since they involve N_0^c/N which is now unknown in the intermediate region of temperatures. The only solution is to use the magnetization M , and define T_{c2} as the temperature for which $N_+^c \simeq N_-^c \ll N$, that is

$$k_B T_{c2} = \frac{2\pi\hbar^2}{mL^2} \left(\frac{M}{g_{\frac{3}{2}}(1) - g_{\frac{3}{2}}(e^{-\frac{2qh^2}{kT_{c2}}})} \right)^{\frac{2}{3}}, \quad (41)$$

what is equivalent to $M = M^T(T_{c2})$. This choice is justified in the thermodynamic limit when $N \gg e^{-2\beta qh^2}/(1 - e^{-2\beta qh^2})$, and mathematically within our equations for $\beta qh^2 \gg 1$ and any N .

Below T_{c2} , condensate fractions satisfy the set of equations:

$$\begin{aligned} N^c &= N - \left(\frac{L}{\lambda_{dB}} \right)^3 \left[2g_{\frac{3}{2}}(1) + g_{\frac{3}{2}}(e^{-2\beta qh^2}) \right], \\ N_+^c - N_-^c &= M^c(T), \\ \frac{2}{N_0^c} &= \frac{1}{N_+^c} + \frac{e^{-2\beta qh^2}}{N_-^c} - 2 \sinh(\beta qh^2) e^{-\beta qh^2}. \end{aligned} \quad (42)$$

Different from (32) is the first equation of (42) only.

B. Phase diagram

The non-zero magnetic field changes dramatically the phase diagram of the critical temperatures, which is shown in Fig. 1. The phase diagram consists of four

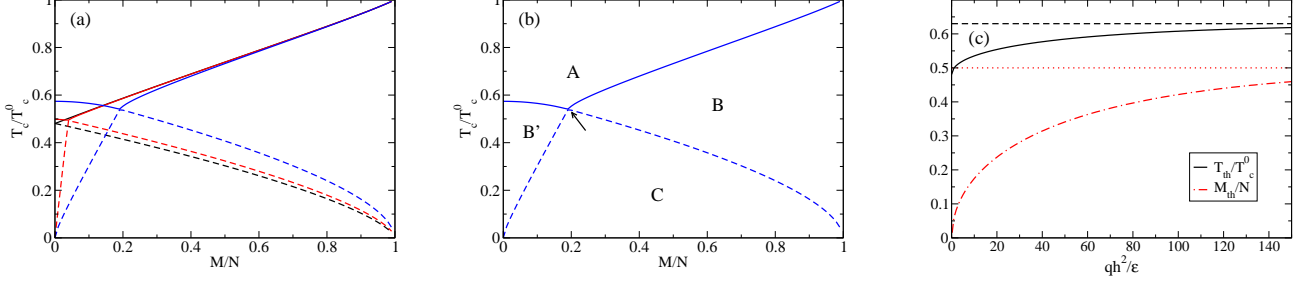


FIG. 1. (Color online) (a) and (b) show the phase diagram of the critical temperatures. T_{c1} is marked by solid lines and T_{c2} is marked by dashed lines. In (a) black lines are for $qh^2 = 0$, red lines are for $qh^2 = 0.5\hbar^2/mL^2$ and blue lines are for $qh^2 = 12.5\hbar^2/mL^2$. $T_c^0 = (2\pi\hbar^2/mL^2)(N/\zeta(3/2))^{2/3}$ is the critical temperature for one component condensate in the box potential. In (b) the same for $qh^2 = 12.5\hbar^2/2mL^2$. The arrow indicates the threshold at the critical temperatures intersection point. Particular parts of the diagram are "A"-thermal atoms (no condensate), "B"-condensate in the component $m_F = 1$, "B'"-condensate in the component $m_F = 0$ only, "C"-condensate possible in all components. (c) The threshold temperature T_{th}/T_c^0 (solid line) and the threshold magnetization M_{th}/N (dash-dotted line) at the critical temperatures intersection point as a function of the quadratic Zeemann energy shift qh^2/ϵ with $\epsilon = \hbar^2/2mL^2$. The asymptotic values of the threshold critical temperature $T_{th}^\infty/T_c^0 = 2^{-2/3}$ and the threshold magnetization $M_{th}^\infty = 1/2$ are marked by dashed and dotted lines respectively. Here, the total number of atoms is $N = 10^4$.

phases "A", "B", "B'", "C" separated by the two critical temperatures T_{c1} and T_{c2} . Depending on the value of the temperature, the system can be: "A"- a non-degenerate thermal gas, "B"- condensate in the component $m_F = 1$ or "B'"-condensate in the $m_F = 0$ and thermal atoms in other components, "C"- a condensate in $m_F = 0$ and $m_F = 1$ while in the $m_F = -1$ is a gas with non-negligible fraction of atoms in the lowest energy level for $\beta qh^2 \ll 1$, or with negligible fraction of atoms in the lowest energy level for $\beta qh^2 \gg 1$. A possible destination is controlled by the magnetization, with a special role of the threshold magnetization at the critical temperatures intersection point $M_{th} \equiv M(T = T_{c1} = T_{c2})$. If $M < M_{th}$ then to obtain particular quantities, one should use expressions from subsection III A 2, in the opposite case ($M > M_{th}$) from subsection III A 1. The procedure to obtain numerical values for the critical temperatures is explained in Appendix C.

Analytical expressions for the threshold critical temperature T_{th} and the threshold magnetization M_{th} are

$$\left(\frac{T_{th}}{C}\right)^{3/2} = \frac{N}{2g_{3/2}(1) + g_{3/2}(e^{-2qh^2/k_B T_{th}})}, \quad (43)$$

$$\frac{M_{th}}{N} = \frac{3g_{3/2}(1)}{N} \left(\frac{T_{th}}{C}\right)^{3/2} - 1, \quad (44)$$

where $C = \hbar^2/2\pi mL^2 k_B$. The above expressions are obtained by comparing critical temperatures T_{c1} and T_{c2} for both $qh^2 > \eta$ and $qh^2 < \eta$. In fig. 1c we show the threshold critical temperature (43), the threshold magnetization (44) and their asymptotic values for $\beta qh^2 \rightarrow \infty$, they are $T_{th}^\infty/T_c^0 \rightarrow 2^{-2/3}$ and $M_{th}^\infty/N \rightarrow 1/2$ respectively.

C. Condensed fractions

Condensate fractions, solutions of equations (32) for $M > M_{th}$ and solutions of equations (42) for $M < M_{th}$, are presented in fig. 2 and 3 respectively and they are marked by lines. Points are results of the Metropolis algorithm adapted to the model (more details concerning the algorithm can be found in section IV B).

Figure 2 is for values of the magnetic field in the area $M > M_{th}$ where $qh^2 \leq \eta$. These graphs show that modifications of condensed fractions occur mainly for low magnetic fields. The effect of the non-zero magnetic field is the most visible on the condensate fraction in the $m_F = -1$ component. Notice, at zero magnetic field the fraction of the condensate in the $m_F = -1$ component decreases simply with the temperature, see fig. 2a. In the transient magnetic field regime, the condensed fraction in the $m_F = -1$ component increases from zero, reaches a maximum and then decreases to zero at the second critical temperature, see fig. 2b. The condensed fraction in the $m_F = -1$ component decreases quickly and can be neglected in the high magnetic field regime, see fig. 2c. Condensed fractions are linked together, when the condensed fraction of the $m_F = -1$ component disappears, in the meantime the condensed fraction in the $m_F = 1$ component decreases and the condensate fraction in the $m_F = 0$ increases. Nevertheless, the slope-breaking that occurs at T_{c2} , already present when $h = 0$, is still neat. The fugacity varies dramatically near the zero temperature for small values of magnetic fields, what explains sharp variations of the condensed fractions in fig. 2b.

Figure 3 is for the magnetization $M < M_{th}$ where $qh^2 \geq \eta$. The value of magnetization is $M = 50$ and is very small as compared to $N = 10^4$, therefore the difference between N_+^c and N_-^c is not visible. Notice, strong

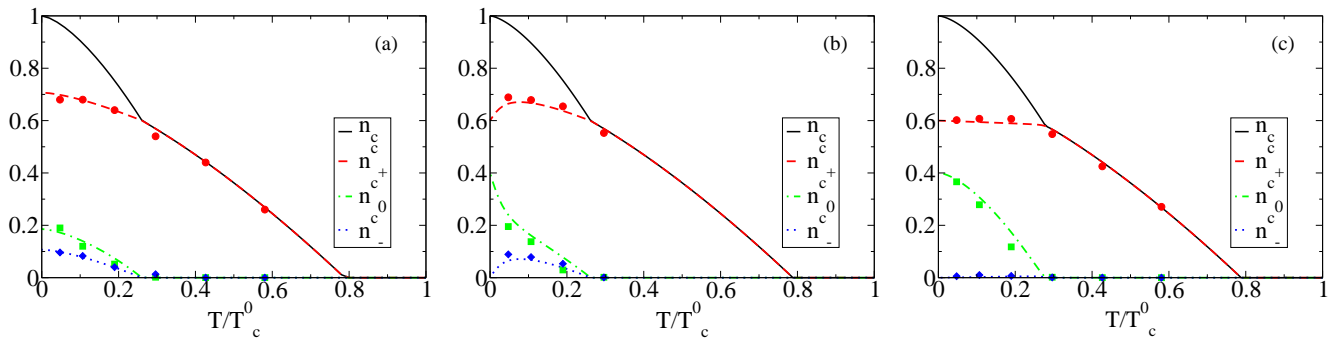


FIG. 2. (Color online) Condensate fractions for $M > M_{th}$, with $N = 10^4$ and $M = 6 \times 10^3$; (a) $qh^2 = 0$, (b) $qh^2 = 0.1 \hbar^2/mL^2$ and (c) $qh^2 = \hbar^2/mL^2$. $n_c = N^c/N$ is the total condensate fraction (solid black line), n_c^+ is the condensate fraction in $m_F = 1$ component (dashed red line), and n_c^0 , n_c^- in $m_F = 0$ (dot-dashed green line), $m_F = -1$ (dotted blue line) respectively. Lines are the solution of equations (32) while points are results of Monte Carlo simulations.

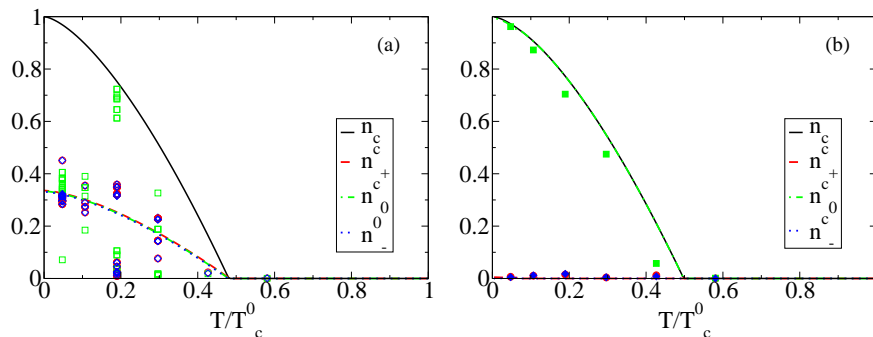


FIG. 3. (Color online) Condensate fractions for $M < M_{th}$, with $N = 10^4$ and $M = 50$; (a) $qh^2 = 0$ and (b) $qh^2 = \hbar^2/mL^2$. $n_c = N^c/N$ is the total condensate fraction (solid black line), n_c^+ is the condensate fraction in the $m_F = 1$ component (dashed red line), and n_c^0 , n_c^- in $m_F = 0$ (dot-dashed green line), $m_F = -1$ (dotted blue line) respectively. Lines are solution of equations (42) while points are results of Monte Carlo simulations. Particular points in (a) correspond to averaging over different representations of an ensemble and show strong fluctuations of condensate fractions in the regime of zero magnetic field and almost zero magnetization.

fluctuations of the condensate fractions for zero magnetic field that are results of Monte Carlo simulations, see different points in fig. 3a. Indeed, for zero magnetization and zero magnetic field the ground state of the ideal gas is strongly degenerate [11], what gives rise to strong fluctuations of condensate fractions. The non-zero magnetic field reduces degeneracy and hence reduces fluctuations of condensate fractions in fig. 3b.

IV. THE INTERACTING GAS

The ground state of a spin-1 Bose gas in the presence of ferromagnetic and antiferromagnetic interactions was widely studied within the single-mode approximation [21] and beyond [22], and was investigated in experiments for antiferromagnetic condensates [8]. The structure of the ground state is quite complex and depends not only on the magnetization and magnetic field but also on the relative phase between components of the Bose gas. It consists of a polar, nematic or magnetic state, two component or three component solutions with phase and anti-

phase matching for ferromagnetic and antiferromagnetic interactions respectively. We are aware of the temperature dependence of such structures, in particular the boundaries between different phases.

The non-zero temperature introduces a multi-mode structure, therefore we describe the system within the classical fields approximation that takes into account thermal populations and interactions among many modes. Indeed, classical fields and stochastic methods [23] as well as Hartree-Fock or Hartree-Fock-Popov approximations [24] were applied for spinor condensates at non-zero temperature but for free magnetization. Among all of finite temperature methods that are used for single-component condensates, the classical fields-like are not perturbative and thus contain all nonlinear terms that are present in the Hamiltonian. It makes them very suitable for study thermodynamics in the whole temperature range, what is not a case for methods based on the Bogoliubov approximation.

Below we just briefly remind the main concept of the classical field approach, more details concerning the foundations of the approximation can be found in [13].

A. The classical fields approximation

The classical fields approach consists of (i) replacement of the creation and annihilation operators by complex amplitudes, (ii) restriction of the summation over modes to a finite number extended all the way to the momentum cut-off \mathbf{K}_{max} .

The field operator is replaced by a classical field (complex function) of well-defined number of momenta modes:

$$\psi_j(\mathbf{r}) = \sum_{\mathbf{k} \leq \mathbf{K}_{max}} a_j(\mathbf{k}). \quad (45)$$

The energy E_ψ of such a classical field is given by discretization of the hamiltonian $H = H_0 + H_A$, eqs. (1) and (2). The total number of atoms is

$$N = \sum_j \sum_{\mathbf{k} \leq \mathbf{K}_{max}} |a_j(\mathbf{k})|^2 \quad (46)$$

and the magnetization is

$$M = \sum_{\mathbf{k} \leq \mathbf{K}_{max}} (|a_+(\mathbf{k})|^2 - |a_-(\mathbf{k})|^2). \quad (47)$$

Various observables have a more or less pronounced dependence on the cut-off. Here we choose the cut-off momentum such, that in the thermodynamic limit the non-condensed density for a single component ideal Bose gas in degenerate regime is exactly reproduced by the classical field model [25]. The condition gives $E_{\mathbf{K}_{max}} \simeq 2.695 k_B T$, where $E_{\mathbf{K}_{max}} = 3\hbar^2(\pi/L)^2/2m$ is the maximal kinetic energy on the grid.

B. The Metropolis algorithm for a spin-1 Bose gas with fixed magnetization

We adapt the Metropolis scheme [14] to the system of classical fields as described in [15]. The main idea of this Monte Carlo method is to generate a Markovian process of a random walk in phase space. All states of the system visited during this walk become members of the statistical ensemble and are used in ensemble averages.

In order to obtain a statistical average of any observable A :

$$\bar{A}_j = \frac{1}{\mathcal{N}} \sum_{s=1}^{\mathcal{N}} \langle \psi_j^{(s)} | A | \psi_j^{(s)} \rangle \quad (48)$$

one should generate \mathcal{N} copies of the classical fields $\psi_j^{(s)}$. A canonical average is obtained in the limit of $\mathcal{N} \rightarrow \infty$ provided the number of members of the ensemble with energy E_ψ is proportional to the Boltzmann factor $e^{-E_\psi/k_B T}$. This can be achieved in a random walk where a single step of the Markov process is defined as follows:

1. A set of amplitudes $a_j^{(s)}(\mathbf{k})$ determines the state selected to be a member of the canonical ensemble at the s th step of the random walk. The corresponding energy E_ψ of the classical field is calculated according to (1) and (2). As the initial condition ($s = 1$), any state that satisfies the condition of the fixed total number of atoms N and the magnetization M may be chosen as a member of the ensemble.
2. A trial set of amplitudes $\tilde{a}_j^{(s)}(\mathbf{k})$ is generated by a random disturbance of $\tilde{a}_j^{(s)}(\mathbf{k}) = a_j^{(s)}(\mathbf{k}) + \delta_j^{(s)}(\mathbf{k})$ followed by normalization to account the total number of atoms. This way a trial classical field $\tilde{\psi}_j^{(s)}$ is obtained. The corresponding magnetization \tilde{M}_s , energy \tilde{E}_ψ , the energy difference $\Delta_s = E_\psi - \tilde{E}_\psi$, as well as the Boltzmann factor $p_s = e^{-\Delta_s/k_B T}$ are then calculated.
3. If the magnetization \tilde{M}_s of a trial set of amplitudes satisfy $|M - \tilde{M}_s| \leq \delta M$ then $\tilde{a}_j^{(s)}(\mathbf{k})$ can be considered as a new member of the ensemble.
4. A new member of the Markov chain $a_j^{(s+1)}(\mathbf{k})$ is selected according to the following prescription: (i) if $\Delta_s < 0$ then the trial state becomes a new member of the ensemble $a_j^{(s+1)}(\mathbf{k}) = \tilde{a}_j^{(s)}(\mathbf{k})$, (ii) if $\Delta_s > 0$ then a random number $0 < u < 1$ is generated. If $u < p_s$ then the trial state becomes a new member of the ensemble. In the opposite case $u > p_s$, the "initial" state $a_j^{(s)}(\mathbf{k})$ is once more included in the ensemble $a_j^{(s+1)}(\mathbf{k}) = a_j^{(s)}(\mathbf{k})$.

The convergence of the procedure is the fastest when approximately every second trial state becomes a member of the ensemble. This factor depends on the assumed maximal value of displacements $\delta_j^{(s)}(\mathbf{k})$ which can be modified during the walk. The parameter δM should be small enough to ensure almost constant magnetization M . Note, some number of initial members of the ensemble should be ignored in order to avoid an influence of the arbitrarily selected initial state of the system.

In order to demonstrate the validity of the algorithm we compare Monte Carlo simulations with the exact solutions for the ideal gas in figures 2 and 3, and with the approximated Bogoliubov theory for antiferromagnetic condensate in fig.4. In the latter case, analytical solutions are given by the Bogoliubov transformation for antiferromagnetic interactions and are valid in the low temperature limit below the critical magnetic field [26]. Both comparisons are satisfactory what allows to use the algorithm in the wider range of interactions.

C. Numerical results

In figures 5 and 6 we show results of numerical simulations using the Metropolis algorithm. Figure 5 is for

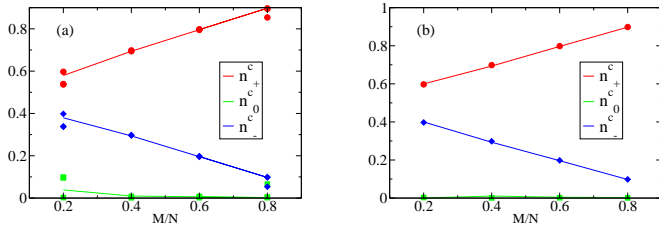


FIG. 4. (Color online) A test of the Metropolis algorithm for ^{23}Na spinor condensate in the low temperature limit. The condensed fractions n_j^c , for $j = \pm, 0$, are plotted in the figure as a function of relative magnetization M/N for (a) $qh^2 = 0$ and (b) $qh^2 = 0.01\hbar^2/mL^2$. Particular colors denote condensate fractions in $m_F = 1$ (red), $m_F = 0$ (green) and $m_F = -1$ (blue) component. Solid lines: the Bogoliubov theory, Points: Monte Carlo results. The total number of atoms is $N = 10^5$.

the magnetization $M = N/2$, and figure 6 for $M = 50$. Condensate fractions for atoms with antiferromagnetic interactions are marked by filled points while for atoms with ferromagnetic interactions by open ones. Particular colored symbols denote condensate fractions in the $m_F = 1$ component (red circles), $m_F = 0$ component (green squares) and in the $m_F = -1$ component (blue diamonds). Solid lines denote results for the ideal gas, added in the figures for comparison.

It clearly reveals the double phase transition that occurs in the system as it is determined by the ideal gas calculations. It does not seem that critical temperatures were affected very much by interactions. Moreover, even condensate fractions for the range of temperatures $T \in [T_{c2}, T_{c1}]$ and any magnetic field follow the ideal gas prediction. It is not very surprising since the system condenses in this regime like the single component gas. Below the second critical temperature the condensate scenario results from the competition between spin-dependent interactions (dominant at low magnetic fields) and the quadratic Zeeman energy (dominant at large magnetic fields). The impact imposed by interactions is the most visible in the low magnetic field regime where ferromagnetic atoms condense differently than antiferromagnetic, and both do not match the ideal gas curve, see figs. 5a and 5b. Nevertheless, dissimilarity in populations of a given component between both interaction types is not so large.

The antiferromagnetic interaction reduces the condensate population in the $m_F = 0$ component in all temperature range for magnetic fields below its critical value known from the ground state analysis [21], see fig. 5a. Simultaneously, the condensate fraction in the $m_F = \pm 1$ components decreases like $(T/T_c^0)^{3/2}$. The ferromagnetic interaction allows for condensation in all components, and populations in the lowest momentum mode may decrease or increase up to the second critical temperature depending on m_F . In the other parameters regime condensate fractions may not simply decay with the tem-

perature but may also increase up to some temperature, reach a maximum and then decrease, see filled red points in fig. 5b for example. This feature is also observed for the ideal gas. In the high magnetic field regime, where the quadratic Zeeman energy dominates over the spin-dependent interaction energy, the condensate scenario matches the ideal gas prediction for both types of interactions, what can be seen in figures 5c and 6b.

The interesting case of almost zero magnetization and zero magnetic field is presented in fig. 6a. We observe strong fluctuations of condensed fractions for atoms with antiferromagnetic interactions (shown in the inset), what is not the case for ferromagnetic atoms (shown in the main window). In the inset of fig. 6a numerous points are obtained by averaging over different representations of ensemble members. Results of the Monte Carlo simulations strongly fluctuate, and additionally they are sensitive to the parameters of simulations (members of ensemble, or δM for example). Similarly as for the ideal gas, the ground state of the antiferromagnetic condensate is degenerated what gives rise to observed fluctuations. The phenomenon that is behind this effect is called spin fragmentation and was already investigated theoretically for the antiferromagnetic spinor condensate [27].

V. SUMMARY

In summary, we have studied the thermodynamics of a spin-1 Bose gas with fixed magnetization in the presence of a non-zero magnetic field. We have given explicit expressions for the two critical temperatures and all condensate fractions for the ideal gas. We have shown the occurrence of a new phase in the phase diagram of critical temperatures. The interacting gas was studied within the classical fields approach, that is not perturbative and includes all nonlinear terms present in the hamiltonian. An alternative method, namely stochastic Projected Gross-Pitaevskii equation, was lately adapted to the case of a spin-1 Bose gas but for free magnetization [23]. We find that interactions strongly affect the condensation scenario below the second critical temperature and for low magnetic fields. In this regime of parameters the thermodynamics of ferromagnetic and antiferromagnetic gases are different. The condensation is not affected much by interactions for values of temperatures between the two critical temperatures $T \in [T_{c1}, T_{c2}]$ for all values of magnetic fields. Furthermore, the condensation is not affected by interactions in the whole temperatures range in the high magnetic field limit. Generalization to a Bose gas with arbitrary spin F is straightforward. Our results open the path to study the influence of a multi-mode structure on the properties of spinor condensates, providing an interesting direction for a future work.

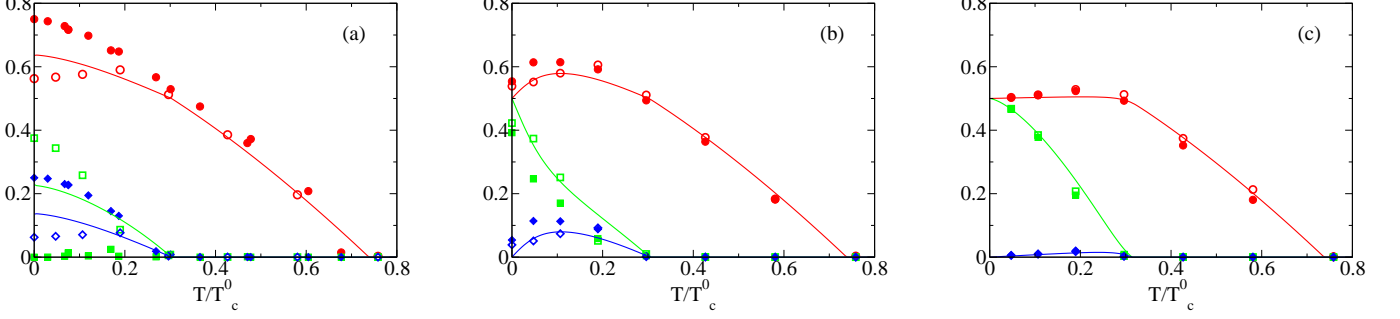


FIG. 5. (Color online) Condensate fractions for ^{23}Na atoms with antiferromagnetic interactions (filled points) and for ^{87}Rb atoms with ferromagnetic interactions (open points). Particular colored symbols denote condensate fractions in the $m_F = 1$ component (red circles), $m_F = 0$ component (green squares) and in the $m_F = -1$ component (blue diamonds). Solid lines are results for the ideal gas. The total number of atoms is $N = 10^4$, the magnetization $M = N/2$ and values of magnetic fields are (a) $qh^2 = 0$, (b) $qh^2 = 0.124 \hbar^2/mL^2$ and (c) $qh^2 = \hbar^2/mL^2$.

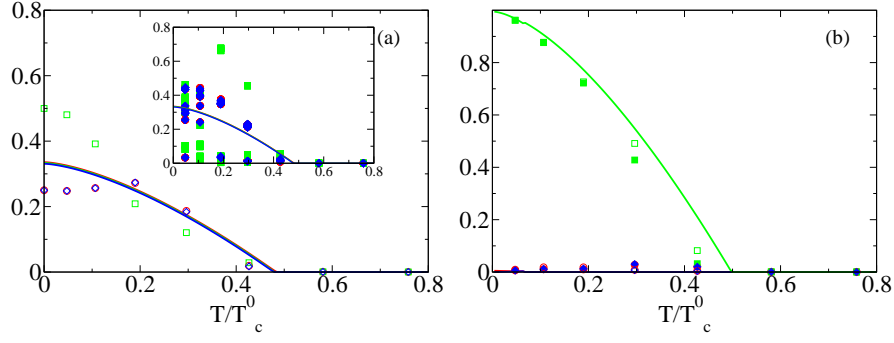


FIG. 6. (Color online) The same as in fig. 5 but for magnetization $M = 50$. Condensate fractions for ^{23}Na atoms with antiferromagnetic interactions are marked by filled points and for ^{87}Rb atoms with ferromagnetic interactions by open points. Particular colored symbols denote condensate fractions in the $m_F = 1$ component (red circles), $m_F = 0$ component (green squares) and in the $m_F = -1$ component (blue diamonds). Solid lines are results for the ideal gas. The total number of atoms is $N = 10^4$ and the values of magnetic fields are (a) $qh^2 = 0$ and (b) $qh^2 = \hbar^2/mL^2$. In (a) condensed fractions for atoms with ferromagnetic interactions are presented in the main window. Numerous points in the inset show condensate fractions for atoms with antiferromagnetic interactions that are obtained by averaging over different representations of ensemble members.

ACKNOWLEDGMENTS

We thank M. Gajda and M. Matuszewski for useful discussions and O. Hul for a careful reading of the manuscript. This work was supported by DEC-2011/03/D/ST2/01938.

Appendix A: Equations for condensate fractions when $T \in [0, T_{c2}]$

Here we show how to obtain equations (32) for condensed fractions.

The first one is obtained by writing $N_c = N_+^c + N_0^c + N_-^c = N - N^T$ in the following

$$N^c = N - \left(\frac{L}{\lambda_{dB}} \right)^3 \left(2g_{\frac{3}{2}}(1) + g_{\frac{3}{2}}(e^{-2\beta qh^2}) \right), \quad (\text{A1})$$

then after introducing $G_{\frac{3}{2}}$ and M^T it has a form

$$N^c = N - M^T(T) - \left(\frac{L}{\lambda_{dB}} \right)^3 G_{\frac{3}{2}}(T). \quad (\text{A2})$$

Knowing that $N - M = (L/\lambda_{dB})^3 G_{\frac{3}{2}}(T)$, after some algebra one finds the first equation of (32).

The second equation of (32) is just rewriting the total magnetization in terms of its condensate and thermal parts $M = (N_+^c - N_-^c) + (N_+^T - N_-^T)$, and an observation that the whole thermal part simply reduces to $M^T(T)$.

The third formula of (32) is a bit more tedious to obtain. It is a peculiar case of a more general formula, valid in any regime, that we shall prove now. Starting from the set of equations

$$N_+^c = \frac{z_+}{1 - z_+}, \quad (\text{A3})$$

$$N_0^c = \frac{z_0}{1 - z_0} = \frac{z_+ z_\eta e^{\beta q h^2}}{1 - z_+ z_\eta e^{\beta q h^2}}, \quad (\text{A4})$$

$$N_-^c = \frac{z_-}{1 - z_-} = \frac{z_+ z_\eta^2}{1 - z_+ z_\eta^2}, \quad (\text{A5})$$

one rewrites

$$\frac{1}{N_+^c} = \frac{1}{z_+} - 1, \quad (\text{A6})$$

$$\frac{1}{N_0^c} = \frac{1}{z_+ z_\eta e^{\beta q h^2}} - 1, \quad (\text{A7})$$

$$\frac{1}{N_-^c} = \frac{1}{z_+ z_\eta^2} - 1, \quad (\text{A8})$$

which shows that

$$\frac{z_\eta e^{-\beta q h^2}}{N_-^c} + \frac{z_\eta^{-1} e^{-\beta q h^2}}{N_+^c} = \frac{2}{N_0^c} + 2 - z_\eta e^{-\beta q h^2} - z_\eta^{-1} e^{-\beta q h^2}, \quad (\text{A9})$$

and it leads to the third equation of (32) in the limit $z_\eta \rightarrow e^{-\beta q h^2}$.

Appendix B: The analytical solution of equations for condensate fractions when $T \in [0, T_{c2}]$

The algebraic considerations of (32) lead to the following equation for N_0^c :

$$N_0^{c3} + a N_0^{c2} + b N_0^c + c = 0, \quad (\text{B1})$$

where

$$a \equiv \frac{1 - 2u N_c + 2\tilde{u}}{u}, \quad (\text{B2})$$

$$b \equiv -\frac{2N_c \tilde{u} - 2M_{eff} u + 2N_c - u N_c^2 + u M_{eff}^2}{u}, \quad (\text{B3})$$

$$c \equiv \frac{N_c^2 - M_{eff}^2}{u}, \quad (\text{B4})$$

and $u(q, h, T) \equiv \sinh(\beta q h^2) e^{-\beta q h^2}$, $\tilde{u}(q, h, T) \equiv \cosh(\beta q h^2) e^{-\beta q h^2}$.

The quadratic Zeeman effect transformed the equation for N_0^c which was a second degree polynomial for the zero magnetic field, into a third degree polynomial. That polynomial has three roots. One needs to select, among those solutions, the only one that is physical: real, non-negative, and with values between 0 and N . To avoid numerical difficulties, one can find analytical solutions of this equation using for instance Cardan's method, and

select the one that has the proper limit when $q h^2 \rightarrow 0$. To do it one defines:

$$X \equiv N_0^c + \frac{a}{3}, \quad (\text{B5})$$

which allows to put the polynomial into the form:

$$X^3 + \tilde{p}X + \tilde{q} = 0 \quad (\text{B6})$$

with

$$\tilde{p} \equiv b - \frac{a^2}{3}, \quad (\text{B7})$$

$$\tilde{q} \equiv \frac{a}{27}(2a^2 - 9b) + c. \quad (\text{B8})$$

Then, one writes:

$$X \equiv u + v, \quad (\text{B9})$$

and notices that u^3 and v^3 are solutions of

$$X^2 + \tilde{q}X - \tilde{p}^3/27 = 0. \quad (\text{B10})$$

Then one introduces

$$\Delta \equiv \frac{27\tilde{q}^2 + 4\tilde{p}^3}{27}. \quad (\text{B11})$$

Numerically, it appears that $\Delta < 0$ and $\tilde{p} < 0$, which means that there are three solutions:

$$X_k = 2\sqrt{-\tilde{p}/3} \cos\left(\frac{1}{3} \arccos\left(-\frac{\tilde{q}}{2}\sqrt{\frac{27}{-\tilde{p}^3}}\right) + \frac{2k\pi}{3}\right), \quad (\text{B12})$$

where $k \in \{0, 1, 2\}$. To find N_{0k}^c , one has to keep in mind that

$$N_{0k}^c = X_k - \frac{a}{3}. \quad (\text{B13})$$

Eventually, one finds that N_{01}^c should always be selected for N_0^c because it is the only solution that gives the appropriate limit when $q h^2 \rightarrow 0$. Then, having N_0^c , one can easily calculate N_+^c , N_-^c with the first and second equations of (32).

Appendix C: How to obtain the phase diagram

In this appendix we explain how to compute numerically the transition temperatures T_{c1} and T_{c2} for any fixed magnetization.

There is an additional difficulty to compute T_{c1} compared to the case when $h = 0$, since its definition involves $z_{\eta c1} \equiv z_\eta(T_{c1})$, which is unknown. One can determine $z_{\eta c1}$ from the constant of motion M/N , but to do so, one has to know the value of T_{c1} , as can be seen from the following sets of equations:

$$T_{c1} \equiv C \left(\frac{N}{F_{\frac{3}{2}}^+(T_{c1}, z_{\eta c1})} \right)^{\frac{2}{3}}, \quad (\text{C1})$$

$$\frac{M}{N} = \frac{g_{\frac{3}{2}}(1) - g_{\frac{3}{2}}(z_{\eta c1}^2)}{g_{\frac{3}{2}}(1) + g_{\frac{3}{2}}(e^{\frac{qh^2}{k_B T_{c1}}} z_{\eta c1}) + g_{\frac{3}{2}}(z_{\eta c1}^2)}, \quad (C2)$$

if $qh^2 \leq \eta$, and

$$T_{c1} \equiv C \left(\frac{N}{F_{\frac{3}{2}}^0(T_{c1}, z_{\eta c1})} \right)^{\frac{2}{3}}, \quad (C3)$$

$$\frac{M}{N} = \frac{g_{\frac{3}{2}}(e^{-\frac{qh^2}{k_B T_{c1}}} z_{\eta c1}^{-1}) - g_{\frac{3}{2}}(e^{-\frac{qh^2}{k_B T_{c1}}} z_{\eta c1})}{g_{\frac{3}{2}}(e^{-\frac{qh^2}{k_B T_{c1}}} z_{\eta c1}^{-1}) + g_{\frac{3}{2}}(1) + g_{\frac{3}{2}}(e^{-\frac{qh^2}{k_B T_{c1}}} z_{\eta c1})}, \quad (C4)$$

if $qh^2 \geq \eta$. There are no further independent equations available for those two quantities, so they have to be solved in a self-consistent way.

Let us suppose that the magnetization is such that the system is in the area where $qh^2 \leq \eta$. One knows the value of T_{c1} without magnetic field, and one can sensibly expect that if a magnetic field is switched on, the critical temperature will be of the same order of magnitude as it used to be, so one puts the value of T_{c1} in the absence of any field $qh^2 = 0$ to compute the value of $z_{\eta c1}$, and then puts this value into (C1) to compute the corrected value of T_{c1} , that can be used in (C2) to compute $z_{\eta c1}$. Those operations should be performed as many times as needed to make the effect of the wrong initial value disappear. The convergence is fast, and after few steps one is close to the fixed point for T_{c1} .

One can proceed in the same way using (C3) and (C4) if $qh^2 \geq \eta$, but how is it possible to know at once if one is in this case or in the other? One does not know it, but it is of no importance whatsoever if one uses a little trick familiar to chemists. At the beginning one makes some assumption, and then checks if the computed value $z_{\eta c1}$ is consistent with this guess. If not, then it means that the assumption was wrong, and that the system is in the other area. One should begin calculations again. Numerical problems can occur if one is really near to the border between the two areas, so one needs to be careful.

Eventually, to find the second critical temperature, one computes the only solution of the equation in T_{c2}

$$T_{c2} - C \left(\frac{N - M}{M^T(qh^2, T_{c2}) + 3g_{\frac{3}{2}}(e^{\frac{-2qh^2}{k_B T_{c2}}})} \right)^{\frac{2}{3}} = 0 \quad (C5)$$

if $qh^2 \leq \eta$, or

$$T_{c2} - C \left(\frac{M}{g_{\frac{3}{2}}(1) - g_{\frac{3}{2}}(e^{\frac{-2qh^2}{k_B T_{c2}}})} \right)^{\frac{2}{3}} = 0 \quad (C6)$$

if $qh^2 \geq \eta$. The bisection method allows to find this value with the requested accuracy, taking 0 for the lower bound and the temperature T_{c1} for the upper bound.

-
- [1] D. M. Stamper-Kurn and M. Ueda, *Rev. Mod. Phys.* **85**, 1191 (2013).
- [2] Y. Kawaguchi and M. Ueda, *Phys. Rep.* **520**, 253 (2012).
- [3] Z. Zhang and L.-M. Duan, *Phys. Rev. Lett.* **111**, 180401 (2013).
- [4] M.-S. Chang, Q. Qin, W. Zhang, L. You and M. S. Chapman, *Nature Physics* **1**, 111 (2005). W. Zhang, D. L. Zhou, M.-S. Chang, M. S. Chapman and L. You, *Phys. Rev. A* **72**, 013602 (2005). C. S. Gerving, T. M. Hoang, B. J. Land, M. Anquez, C. D. Hamley and M. S. Chapman, *Nature Communications* **3**, 1169 (2012).
- [5] T. M. Hoang, C. S. Gerving, B. J. Land, M. Anquez, C. D. Hamley and M. S. Chapman, *Phys. Rev. Lett.* **111**, 090403 (2013).
- [6] C. D. Hamley, C. S. Gerving, T. M. Hoang, E. M. Bookjans and M. S. Chapman, *Nature Physics* **8**, 305 (2012).
- [7] J. Guzman, G.-B. Jo, A. N. Wenz, K. W. Murch, C. K. Thomas, and D. M. Stamper-Kurn, *Phys. Rev. A* **84**, 063625 (2011).
- [8] D. Jacob, L. Shao, V. Corre, T. Zibold, L. De Sarlo, E. Mimoun, J. Dalibard and F. Gerbier, *Phys. Rev. A* **86**, 061601 (2012). J. Jiang, L. Zhao, M. Webb, and Y. Liu, *Phys. Rev. A* **90**, 023610 (2014).
- [9] T. Isoshima, T. Ohmi and K. Machida, *J. Phys. Soc. Jpn.* **69**, 3864 (2000).
- [10] Y. M. Kao and T. F. Jiang, *Eur. Phys. J. D* **40**, 263 (2006).
- [11] W. Zhang, S. Yi and L. You, *Phys. Rev. A* **70**, 043611 (2004).
- [12] B. Pasquiou, G. Bismut, Q. Beaufils, A. Crubellier, E. Marechal, P. Pedri, L. Vernac, O. Gorceix and B. Laburthe-Tolra, *Phys. Rev. A* **81**, 042716 (2010). B. Pasquiou, E. Marechal, L. Vernac, O. Gorceix and B. Laburthe-Tolra, *Phys. Rev. Lett.* **108**, 045307 (2012).
- [13] Y. Kagan, B. V. Svistunov, *Phys. Rev. Lett.* **79**, 3331 (1997). M. J. Davis, S. A. Morgan and K. Burnett *Phys. Rev. Lett.* **87**, 160402 (2001). A. Sinatra, C. Lobo, Y. Castin, *Phys. Rev. Lett.* **87**, 210404 (2001). K. Goral, M. Gajda, K. Rzażewski, *Opt. Express* **8**, 92 (2001). M. Brewczyk, P. Borowski, M. Gajda, K. Rzażewski, *J. Phys. B* **37** 2725 (2004).
- [14] N. Metropolis et al., *J. Chem. Phys.* **21** 1087 (1953).
- [15] E. Witkowska, M. Gajda, K. Rzażewski, *Optics Communications* **283** 671-675 (2010).
- [16] C. Lobo, A. Sinatra and Y. Castin, *Phys. Rev. Lett.* **92**, 020403 (2004). T. Karpiuk, M. Brewczyk, M. Gajda, K. Rzażewski, *J. Phys. B: At. Mol. Opt. Phys.* **42** No 9 095301 (2009). C. N. Weiler, T. W. Neely, D. R. Scherer, A. S. Bradley, M. J. Davis, and B. P. Anderson, *Nature* **455**, 948 (2008).
- [17] M. J. Davis, S. A. Morgan, *Phys. Rev. A* **68**, 053615 (2003).

- [18] A. Sinatra, E. Witkowska, J.-C. Dornstetter, Yun Li, and Y. Castin, Phys. Rev. Lett. **107**, 060404 (2011). A. Sinatra, Y. Castin, E. Witkowska, Europhysics Letters **102** 40001 (2013).
- [19] E. Witkowska, P. Deuar, M. Gajda, K. Rzażewski, Phys. Rev. Lett. **106**, 135301 (2011). T. Karpiuk, P. Deuar, P. Bienias, E. Witkowska, K. Pawłowski, M. Gajda, K. Rzażewski, M. Brewczyk, Phys. Rev. Lett. **109**, 205302 (2012).
- [20] Finite Temperature and Non-Equilibrium Dynamics, S. Gardiner, N. Proukakis, M. Davis, M. Szymanska editors, Cold Atom Series, 1, Imperial College Press, London 2013.
- [21] J. Stenger, S. Inouye, D. M. Stamper-Kurn, H.-J. Miesner, A. P. Chikkatur and W. Ketterle, Nature **396**, 345 (1998). W. X. Zhang, S. Yi and L. You, New J. Phys. **5**, 77 (2003). K. Murata, H. Saito and M. Ueda, Phys. Rev. A **75**, 013607 (2007). M. Matuszewski, T. J. Alexander and Y. S. Kivshar, Phys. Rev. A **80**, 023602 (2009).
- [22] M. Matuszewski, T. J. Alexander, and Y. S. Kivshar, Phys. Rev. A **78**, 023632 (2008).
- [23] A. S. Bradley and P. B. Blakie, Phys. Rev. A **90**, 023631 (2014).
- [24] N. T. Phuc, Y. Kawaguchi and M. Ueda, Phys. Rev. A **84**, 043645 (2011). Y. Kawaguchi, N. T. Phuc and P. B. Blakie, Phys. Rev. A **85**, 053611 (2012).
- [25] E. Witkowska, M. Gajda, K. Rzażewski, Phys. Rev. A **79** 033631 (2009). A. Sinatra, E. Witkowska, Y. Castin, Eur. Phys. J. Special Topics **203**, 87-116 (2012).
- [26] E. Witkowska, J. Dziarmaga, T. Świsłocki, M. Matuszewski, Phys. Rev. B **88**, 054508 (2013).
- [27] L. DeSarlo, L. Shao, V. Corre, T. Zibold, D. Jacob, J. Dalibard, F. Gerbier, New J. Phys. **15** 113039 (2013).